Journal of Applied Fluid Mechanics, Vol. 18, No. 10, pp. 2465-2475, 2025.
Available online at www.jafmonline.net, ISSN 1735-3572, EISSN 1735-3645.
https://doi.org/10.47176/jafm.18.10.3538

Investigating the Effect of Grooves on the Hydraulic Parameters of a Sharp-crested Trapezoidal Side Weir

R. Daneshfaraz[1,2†], E. Aminvash[3], R. Omidvar[1], V. Süme[2], H. O. Marangoz[2] and E. Yılmaz[2]

[1] *Department of Civil Engineering, Faculty of engineering, University of Maragheh, Maragheh, East Azerbaijan, Iran*
[2] *Department of Civil Engineering, Faculty of Engineering and Architechture, Recep Tayyip Erdoğan University, Rize, Turkey*
[3] *Faculty of Civil Engineering, University of Tabriz, Tabriz, East Azerbaijan, Iran*

†*Corresponding Author Email: daneshfaraz@maragheh.ac.ir*

ABSTRACT

This study investigates the impact of groove implementation on the hydraulic performance of sharp-edged trapezoidal side weirs, focusing on discharge coefficients and shear stress behavior. The simulation processes were carried out using the VOF (Volume of fluid) methodology in combination with the RNG (Re-normalize group) model for turbulence. The validation with experimental data by comparison showed that the relative error in the range of 0.4-2.6%. It was found from the results that the discharge coefficient increases in the no-grooved model and decreases in the grooved model. The identified variation of the discharge coefficient range through different Froude numbers lies between 0.6 and 0.8, where the discharge coefficient of the no-grooved model is larger by 2.68% compared to that of the grooved model. The grooved model was more effective for lower flow rates, while the no-grooved model was more effective for higher flow rates. In all cases, in both models, the discharge coefficient increases with the Froude number, with a greater increase observed in the no-grooved configuration (19.64% higher). The research indicated that grooves significantly reduce shear stresses at the crest of the weir, reducing further damage to the structure. The variation in shear stress between the two models was most evident under high flow conditions, demonstrating the efficiency of the grooved model in reducing harmful stresses and energy dissipating.

Article History

Received March 24, 2025
Revised April 22, 2025
Accepted May 27, 2025
Available online August 5, 2025

Keywords:

Discharge coefficient
Froude number
Grooves
Shear stress
Supercritical flow

1. INTRODUCTION

Side weirs are spillway protection mechanisms used in a variety of water transportation systems. Commonly, these hydraulic structures operate in a regime of variable free flow characterized by a downstream reduced discharge near a main channel. In applications pertaining to side weirs, water is spilled out of the main channel, resulting in reduced flow in the reach downstream. The present research focuses on exploring changes in the geometry that affect hydraulic properties of fluid flow in trapezoidal side weir. Research on sharp-edged side weir has yielded a set of different results in which scholars have also suggested various equations for the respective hydraulic parameters. More importantly, De Marchi (1934) managed to formulate a relationship to determine the value of the water passage coefficient for a unit width of side weir.

$$C_d = \frac{3q}{2\sqrt{2g} \times (h-p)^{\frac{3}{2}}} \quad (1)$$

In the above equation, h is the water depth in the main channel, P is the height of the side weir, C_d is the discharge coefficient of the passing flow, g is the gravitational acceleration, and q is the unit discharge per width. Singh et al. (1994), through experimental studies on the flow discharge coefficient, found that this coefficient depends on factors such as the ratio of weir height to upstream flow depth and the Froude number. They presented the following equation for the flow discharge coefficient:

$$C_d = 0.33 - 0.18Fr_1 + 0.49\frac{p}{y_1} \quad (2)$$

where P is the crest height of the weir, y_1 is the upstream water depth, Fr_1 is the Froude number, and C_d is the discharge coefficient.

The hydraulic and geometric properties have been the subject of an in-depth study by many scholars for a side weir. One of the fundamental works in this area has been carried out by Hager (1987), who investigated the flow depth, velocity of flow, angle of exit, and structure of the

side weir parameters that play a significant role in affecting the process of flow discharge.

Several factors influence the flow characteristics over side weirs: the flow conditions both in the approach flow upstream of the main channel and downstream of the side weir. The longitudinal profile over a side weir is generally divided into three classes by the Froude number, which are: subcritical, supercritical, and critical. Durga Rao and Pilla (2008) investigated the application of the momentum principle to the study of spatially varied flow taking place under supercritical conditions and demonstrated thereby that the fluctuation in the side weir discharge coefficient was a function of the Froude number. Hyung and Sop (2010) performed an experimental investigation on the influence of the upstream Froude number, the weir dimensions (height, length, and width), and principal channel width on the flow discharge coefficient in the case of broad-crested side weirs located in a wide rectangular channel. The results of this study showed that for subcritical flow and Froude numbers less than unity, the relative height and the relative length of weir are gaining importance.

Aydin and Emiroglu (2013) discretized the governing equations using the finite volume approach to investigate the discharge coefficient for a flow over a side labyrinth weir. Their results showed that variations in crest height, weir width, and side slope were in good agreement for various supercritical and subcritical flow conditions when their results were compared with experimental models as well as numerical solutions. Tabrizi et al. (2015) conducted an experimental study on the discharge coefficient and relevant parameters of trapezoidal side weirs that were in different crest lengths, heights, and wall slopes. The results obtained from this study showed that the discharge coefficient of sharp-crested trapezoidal weirs is variable and depends on many factors that have been involved in hydraulic conditions of flow in the upstream of the weir and flow cross-section passing over the weir. The authors synthesized the pre-existing equations from the research conducted by Henderson (1966) and those proposed by Kumar and pahtak (1987) into the following equation for sharp-crested trapezoidal weir:

$$\frac{dQ}{dx} = -\frac{14}{16} C_M \sqrt{2g} (y - p)^{1.5} \tag{3}$$

Abdollahi et al. (2017) studied flow passing over the side labyrinth weirs using some obstacles. This study demonstrated that the maximum discharge in the side labyrinth weirs occurs when the obstacles are located perpendicular to the flow path and downstream of the weir. Seyedjavad et al. (2019) conducted an experimental study about the discharge coefficient of trapezoidal piano key side weirs, stating that this particular structure acts with better performance than its triangular and trapezoidal labyrinth counterparts. Furthermore, Jalili Ghazizadeh et al. (2021) investigated the characteristics of the water surface profile over rectangular side weirs in supercritical flow conditions. The authors have proposed a new equation to determine the discharge in the main channel next to the side weir. Comparing the analyses of the proposed equations with various sets of available experimental data has shown that these equations can predict the water surface profile and flow discharge quite accurately. Kalateh et al. (2024a) and Kalateh and Aminvash (2023) studied the flow surface profile passing a sharp-crested rectangular side weir at various bed slopes and found out that for a constant slope, the water surface profile increases from inlet to outlet of the weir for subcritical flow regime, and it decreases for supercritical flow regime. Furthermore, it is mentioned that by steepening the bed slope of the main channel, the flow surface over the weir decreases.

Maranzoni et al. (2017) conducted to experimental and numerical analysis of side weir flows in a converging channel. Results showed that the assumption of constant specific energy usually adopted in one-dimensional side weir flow modeling is reasonably valid, despite the considerable increase in the velocity-head and momentum correction coefficients along the side weir. Nistoran et al. (2023) has done numerical simulation of flow over a side weir for diversion structures and water intake. Results showed that the water surface elevation profile along the weir crest is computed, together with a qualitative comparison between the shape of the simulated flow nappe and in-situ visualizations.

A review of previous studies shows that most studies conducted in the field of side weirs have been limited to experimental models with rectangular geometry and have focused more on the discharge coefficient parameter. Therefore, in the present study, in addition to changing the geometry of side weir to trapezoidal, the effect of the groove on it has also been studied. On the other hand, in addition to studying the discharge coefficient, the effect of the grooves created on the hydraulic jump efficiency downstream of the trapezoidal side weir has been studied for the first time. Side weirs are very useful in the management of discharge and conveyance; their different configurations and various conditions have been the subject of numerous studies. Most of these were experimental, but with the limited laboratories and high costs associated with these, besides advances in numerical methods, the simulation of these weirs using CFD software has become ever so relevant.

2. MATERIALS AND METHODS

In this research, trapezoidal side weirs are numerically simulated by using FLOW-3D software, version 11.0.4. FLOW-3D is a specialized software applied to solve various CFD problems. FLOW-3D includes a comprehensive listing of features, including the solution of Navier-Stokes equations and the possibility for simulation of free-surface flows. The Volume of Fluid method discretizes the flow equations. It discretizes the differential equations and solves them in the small control volume defined throughout the flow field. A great deal of interest has been placed on this method since it provides solutions that are reasonably accurate and stable for fluid problems, including complex and turbulent flows (Daneshfaraz & Ghaderi, 2017).

The general continuity and momentum equations used in this study are presented in Equation 4

(Daneshfaraz et al., 2020 ; Ghaderi et al., 2020; Daneshfaraz et al., 2021a; Aminvash & Roshangar, 2023; Aminvash et al., 2024):

$$\begin{aligned}
&\frac{\partial U_i}{\partial t}+\frac{1}{V_F}\left[uA_x\frac{\partial u}{\partial x}+vA_y\frac{\partial u}{\partial y}+wA_z\frac{\partial u}{\partial z}\right]\\
&\qquad -\xi\frac{A_y v^2}{xV_F}=\\
&-\frac{1}{\rho}\frac{\partial P}{\partial x}+G_x+f_x-\frac{R_{SOR}}{\rho V_F}(u-u_w-\delta u_s)\\
&\frac{\partial U_i}{\partial t}+\frac{1}{V_F}\left[uA_x\frac{\partial u}{\partial x}+vA_y\frac{\partial u}{\partial y}+wA_z\frac{\partial u}{\partial z}\right]\\
&\qquad +\xi\frac{A_y v^2}{xV_F}=\\
&-\frac{1}{\rho}\frac{\partial P}{\partial y}+G_y+f_y-\frac{R_{SOR}}{\rho V_F}(v-v_w-\delta v_s)\\
&\frac{\partial U_i}{\partial t}+\frac{1}{V_F}\left[uA_x\frac{\partial u}{\partial x}+vA_y\frac{\partial u}{\partial y}+wA_z\frac{\partial u}{\partial z}\right]=\\
&-\frac{1}{\rho}\frac{\partial P}{\partial z}+G_z+f_z-\frac{R_{SOR}}{\rho V_F}(w-w_w-\delta w_s)
\end{aligned} \tag{4}$$

where u, v, and w are the velocities in the x, y, and z directions, respectively; p is the kinetic pressure; ρ is the density of water; G_x, G_y, G_z are the volumetric accelerations in the x, y, and z directions, respectively; f_x, f_y, f_z the mass accelerations in the x, y, and z directions, respectively.

In FLOW-3D software, for the simulation of flow by the VOF method, the software offers several turbulence models that one can apply to his model, including but not limited to the following.

1- Large Eddy Simulation (LES)

2- Two-Equation Model (k-ε)

3- RNG Model

4- Prandtl's Mixing Length Model

Different models were used in carrying out the simulation of flow. In the present study, the RNG turbulence model was used because almost all the selected models gave proper results, but due to less error in the output results, this model is used. Corresponding equations that define this method are thus presented. The RNG model gives the explicit calculations for Reynolds renormalization groups. The statistics approach is a basis for the solution in the RNG method. The turbulence quantities in the equations-that govern-the RNG turbulence simulation, including turbulence kinetic energy, *k*, and turbulence dissipation rate, *ε* are presented below:

$$\frac{\partial(\rho k)}{\partial t}+\frac{\partial(\rho k u_i)}{\partial x_i}=\frac{\partial}{\partial x_j}[(\mu+\frac{\mu_t}{\sigma_k})\frac{\partial k}{\partial x_j}]+P_k-\rho\varepsilon \tag{5}$$

$$\frac{\partial(\rho\varepsilon)}{\partial t}+\frac{\partial(\rho\varepsilon u_i)}{\partial x_i}=\frac{\partial}{\partial x_j}[(\mu+\frac{\mu_t}{\sigma_\varepsilon})\frac{\partial\varepsilon}{\partial x_j}]+C_{1\varepsilon}\frac{\varepsilon}{k}P_k-C_{2\varepsilon}^{*}\rho\frac{\varepsilon}{k} \tag{6}$$

where in the above equations:

$$C_{2\varepsilon}^{*}=C_{2\varepsilon}+\frac{C_\mu\eta^3(1-\frac{\eta}{\eta_0})}{1+\beta\eta^3} \tag{7}$$

$$S=\sqrt{2S_{ij}S_{ij}} \tag{8}$$

$$S_{ij}=\frac{1}{2}(\frac{\partial u_i}{\partial x_j}+\frac{\partial u_j}{\partial x_i}) \tag{9}$$

2.1 Dimensional Analysis

Since the discharge coefficient is a function of the geometric characteristics of the structure, it depends from hydraulic properties of the fluid. The discharge coefficient of a side weir can then be expressed as follows, as a function of relevant geometric and hydraulic characteristics:

$$C_d=f_1(y_1,y_2,V_1,V_2,P,B,L,g,T,H,L',n,m,Z,S_0) \tag{10}$$

which can be rewritten using Π-Buckingham's theory:

$$C_d=f_2(Fr_0,Re,We,\frac{y_2}{y_1},\frac{P}{y_1},\frac{B}{y_1},\frac{T}{L},\frac{H}{L'},S_0,n,m,Z) \tag{11}$$

where Fr_0 is the upstream Froude number, Re is the Reynolds number, We is the Weber number, P is the crest height of the weir, $\frac{y_2}{y_1}$ the downstream to upstream depth ratio, $\frac{P}{y_1}$ the ratio of weir height to upstream water depth, $\frac{B}{y_1}$ the ratio of the main channel width to upstream water depth, $\frac{T}{L}$ the ratio of the overflow length to the weir crest length, $\frac{H}{L'}$ the ratio of water height over the weir to the weir crest length, S_0 the channel bed slope, Z is the side slope of the weir, n is the number of teeth, and m is the ratio of each groove's dimension to the weir crest length. Figure (1) shows the geometric parameters of the side weir.

Since more than three centimeters of water depth is flowing on the weir and the boundary layer is negligible, surface tension and viscosity effects can be ignored (Tabrizi et al., 2015). Given that the Reynolds number is in the range of 23408 to 121098 and this range represents the turbulent regime for the Reynolds number, the Reynolds number parameter can be ignored (Ghaderi et al., 2020; Daneshfaraz et al., 2021b; Bagherzadeh et al., 2022). Also, since the length, width, height, and longitudinal slope of the main channel, and the number and dimensional ratios of the teeth are constant; the dependent parameters in terms of function can be expressed by the independent parameters according to Equation 12.

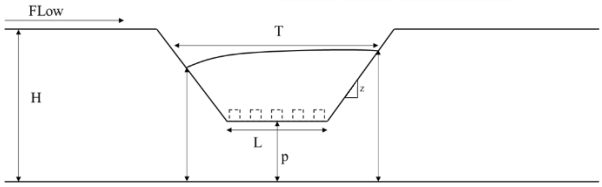

Fig. 1 Schematic of Geometric Parameters

Table 1 Comparison of Experimental and Numerical Data

$\frac{P}{y_1}$	Experimental date (Tabrizi et al., 2015)	Numerical date	MAE	RMSE	R^2
0.681	0.780	0.808	0.014	0.019	0.993
0.694	0.795	0.825	0.015	0.021	0.988
0.712	0.790	0.810	0.009	0.014	0.991
0.739	0.793	0.828	0.175	0.024	0.990
0.743	0.763	0.794	0.015	0.021	0.991
0.759	0.780	0.787	0.003	0.004	0.994
0.778	0.751	0.785	0.017	0.024	0.990
0.791	0.786	0.767	0.009	0.134	0.978
0.810	0.768	0.806	0.019	0.026	0.981
0.825	0.805	0.840	0.017	0.024	0.988
0.841	0.800	0.841	0.021	0.028	0.985

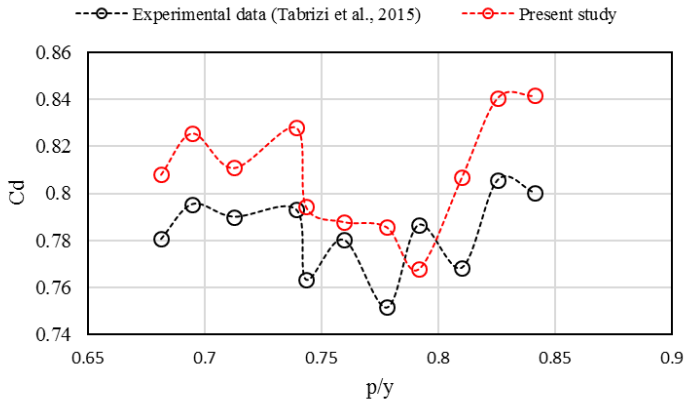

Fig. 2 Comparison Chart of the Discharge Coefficient in the Experimental Model and Numerical Simulation

$$C_d = f_3(Fr_0, \frac{P}{y_1}, \frac{T}{L}) \quad (12)$$

The validation conducted and the results obtained, as represented in Table 1 and Fig. 2 below, serve to compare the values of discharge coefficient obtained from the experimental data of Tabrizi et al. (2015) and those of the numerical data. From this comparison, the values of MAE and RMSE were found to be 0.0287 and 0.0311 percent, respectively. These results therefore show low error and acceptable agreement between the values obtained numerically and experimentally. By performing a validation on the data of Tabrizi et al. (2015) and based on the results presented in Table 1, it can be seen that based on evaluation parameters 1, 2, and 3, the numerical data have a very good agreement with the laboratory data. This is while the numerical data has simulated the laboratory data with a ratio of 0.4% to 2.6%, which are very good results.

2.3 Numerical Simulation

In this research, trapezoidal side weirs are numerically simulated by using FLOW-3D software. In this simulation, a 270 cm length, 30 cm wide and 60 cm height of main channel was considered. It contains a trapezoidal weir in this channel, which has a 30 cm long crest and a height of 20 cm. The side slope will be 1 Besides, there are 5 teeth in the weir's edge, and each of them has a ratio in dimension to weir's crest of 0.1. Based on the trial and error conducted for the simulation duration, in the present study, to achieve steady flow conditions and stabilize the flow, the total simulation duration (Finish time) was considered to be 50 seconds with a simulation time step of 0.01 seconds.

Choosing an appropriate mesh with precision will increase the precision and improve the predictive capability of the simulation results. Therefore, to choose the optimal and exact mesh, various meshes shall be investigated and one should be chosen out based on obtained results. According to the results from Table 2, number 3 mesh was used in the simulation due to the lowest error among other models. Also, about the turbulence models mentioned in Table 4, the RNG model showed the best performance and minimum error compared with other turbulence models; thus, the RNG model has been used in this simulation. It is proper to mention that the other turbulence models gave quite reasonable results, too, with error margins that were acceptable. The process of performing simulations is shown in the flowchart presented in Fig. 3.

To be independent of the mesh, three cell sizes have been used for meshing. In general, two mesh blocks are considered for the solution domain, one for the main channel and the other for the side channel (Table 3). Based on the sensitivity analysis conducted for meshing, a model with a cell size of 1.0 cm for mesh block 1 and 0.5 cm for

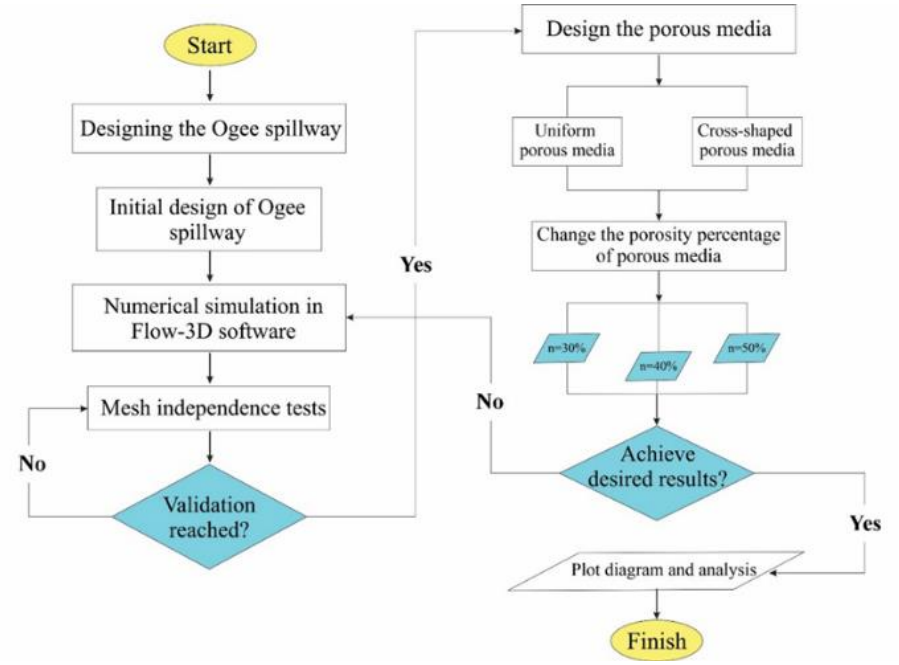

Fig. 3 Flowchart of numerical simulation of present research

Table 2 Evaluation of Error in Different Meshes

Model	Number of Meshes	$E = \left\|\frac{C_{dE} - C_{dN}}{C_{dE}}\right\| \times 100$	MAE	RMSE
Model 1	106440	22.071	0.084	0.121
Model 2	360750	15.579	0.059	0.084
Model 3	2886000	3.891	0.028	0.031

Table 3 Meshing sensitivity analysis on energy dissipation parameter

Model	Size of cells (cm)		Number of Meshes	MAE
	Mesh block 1	Mesh block 2		
Model 1	1.5	0.75	106440	0.084
Model 2	1.2	0.6	360750	0.059
Model 3	1.0	0.5	2886000	0.028

Table 4 Evaluation of Error in Different Turbulence Models

Turbulence Model	Number of Meshes	MAE	RMSE	R^2	NSE
$(k-\omega)$	2886000	0.087	0.038	0.986	0.960
$(k-\varepsilon)$	2886000	0.037	0.028	0.984	0.977
RNG	2886000	0.028	0.031	0.992	0.993

mesh block 2 with a total number of 2886,000 cells was selected for simulation.

The reason for using this turbulence model is its ability to simulate a flow with a large computational mesh, good performance in simulating flow separation, superior results with sudden strain and curvature, as well as success in previous numerical studies (Simsek et al., 2016; Ghaderi et al., 2020; Kalateh et al., 2024b; Kalateh & Aminvash, 2025).

Figure 4 shows the view of the sharp-crested trapezoidal side weir with and without grooves, and Fig. 5 presents the boundary conditions applied in the numerical simulation. Based on Fig. 5, the boundary conditions presented can be summarized in Table 5.

The fluid used in the present study is water, which is an incompressible fluid. Mass flux of material with density ρ (mass per unit volume) is:

$$J_p = \rho v \tag{13}$$

Using either the Eulerian or the Lagrangian time derivatives, mass conservation becomes:

$$\frac{\partial \rho}{\partial t} + \nabla \rho . v = 0 \tag{14}$$

In an incompressible fluid, particles have constant density, and so in the particle frame of reference, the Lagrangian observer does not see any density variation and $D\rho/Dt = 0$. In this case, mass conservation takes the simple form $\nabla \cdot v = 0$, which is commonly called the continuity equation.

Table 5 Boundary conditions

	X direction		Y direction		Z direction	
	X min	X max	Y min	Y max	Z min	Z max
Mesh block 1	VFR	Outflow	Wall			Sym.
Mesh block 2	Sym.		Wall		Sym.	Sym.

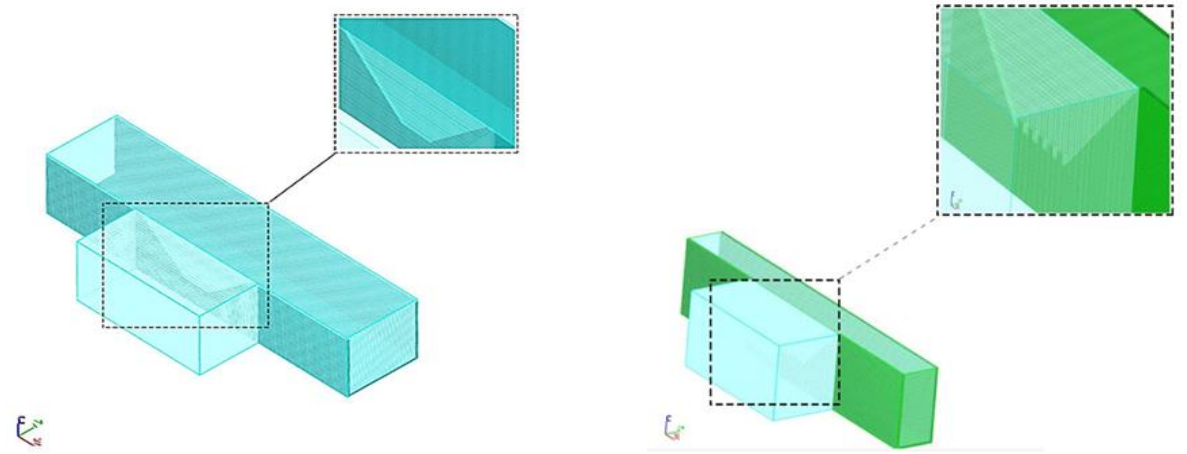

no-grooved **Grooved**

Fig. 4 Comparison of grooved and no-grooved models

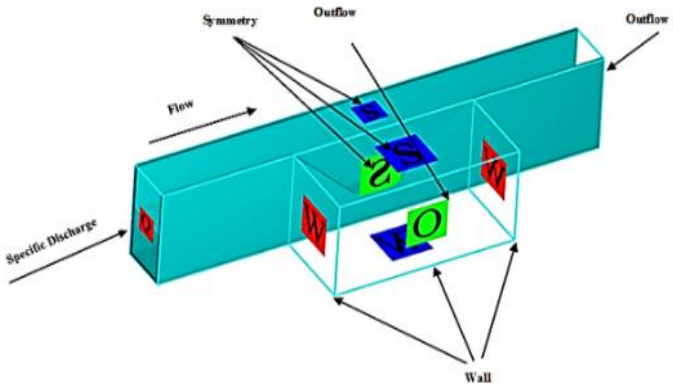

Fig. 5 Boundary Conditions

3. RESULTS AND DISCUSSIONS

In this paper, the variation of C_d with the increasing Froude number is investigated for the two trapezoidal side weir models without and with grooves.

The results provide evidence that the coefficient C_d generally increased in the trapezoidal side weir model with a sharp-crested inlet in view of the rise in the Froude number, as depicted by the upward trend in the graph. This particular trend has been pretty well demonstrated in the model without grooves. Previous experimental investigations have demonstrated that the coefficient C_d increases with the rise in the Froude number in trapezoidal sharp-crested side weirs. In the model without grooves, with the increase in the Froude number, the discharge coefficient increases 25.92% between minimum and maximum discharges. This is because of the increase of energy and hence flow velocity in the no-grooved model for higher discharges, which increases the flow separation area.

Whereas in the grooved model, the coefficient C_d generally shows a trend of decrease with increased Froude number. In this model, the groove came to form obstacles to the flow path, causing a reduction in flow separation area and, as such, reducing the discharge coefficient. For the grooved model, with increased Froude numbers for maximum and minimum discharges, the coefficient C_d was reduced by 22.98%. Generally, the discharge coefficient tends to decrease with more numbers of grooves, and this reduction in discharge coefficient therefore infers that Grooves perform better in the dissipation process and regulating the flow. Figure 6 shows the comparison of discharge coefficients for different Froude numbers for the grooved and no-grooved models.

By comparing the two curves, one can clearly find out the discharge coefficient is 22.22% higher in the no-

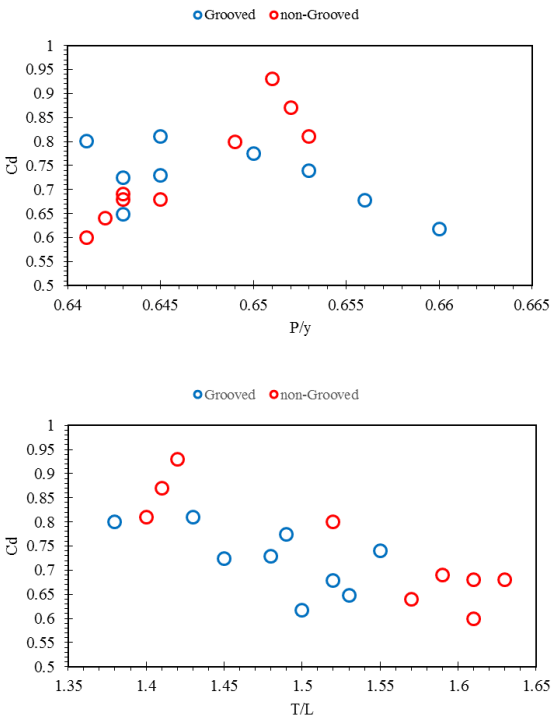

Fig. 6 Comparison and impact of weir geometry on discharge coefficient

grooved model as compared to the grooved model. The results also showed that the grooved model gives better performance in terms of lower Froude numbers whereby the energy and the velocity of flow could be dissipated, whereas the no-grooved model gives better performance at higher Froude numbers where a higher quantity of passing discharge could be provided. In the no-grooved model from Fig. 6(a), the discharge coefficient is observed to increase when the height of the weir increases and also to an increase in diversion flow. This is due to enlargement of the flow separation area caused by the geometry of the no-grooved model. In the case of the no-grooved models, the flow passes over the weir directly without any obstacle. It gives rise to flow separation zones at several points of the weir, which is responsible for enhancing the value of the discharge coefficient.

In the grooved model, however, it can be seen from Fig. 6(b) that the flow separation area has been reduced due to the grooves. The grooves protrude into the path of flow and create turbulence and a deflection of flow that reduces the separation area. This has caused the separation area to be reduced, which consequently reduces energy loss and discharge coefficient. In other words, grooves reduce the discharge coefficient by reducing flow separation and enhancing flow distribution.

These differences in the performance between models with and without grooves indicate that geometrical configuration and design may cause significant effects in the hydraulic performance of a weir. These may lead to an increase in passing flow, increase in flow energy, and velocity downstream of the weir in no-grooved models. Downstream, this may result in serious risks and damages. On the contrary, grooved models contribute to an increase

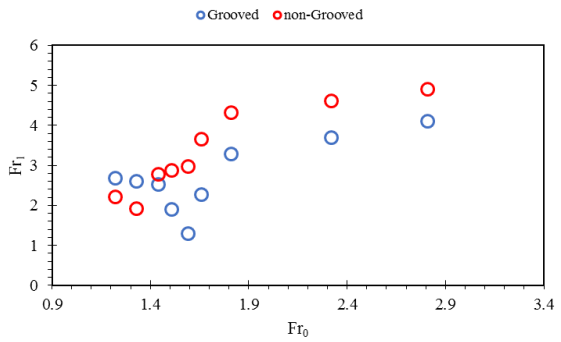

Fig. 7 Examination of the Froude number passing over the weir

in the safety and stability of hydraulic structures by way of better flow control and reduction of the discharge coefficient.

Figure 8 presents the passing Froude number over the weir, Fr_1, against the initial one, Fr_0. For both the grooved and no-grooved weir models, the general increasing trend of the Froude number over the weir with increasing the Froude number is observed. This could be interpreted by the increase in kinetic energy for the incoming flow which surely increases the passing energy over the weir. The calculated Froude number over the weir in the no-grooved model is 19.64% higher than in the grooved model. In the case of groove structures, the energy of flow dissipates more, and thus this could be considered as a fact for giving a reason for the higher value of Froude number in the case of the no-grooved model. This is because the increased passing Froude number relates directly to increased flow velocity and energy that may cause considerable damage and deterioration downstream of the side channel. In other words, flow with high kinetic energy downstream can damage the existing structure or even affect natural formations.

In the grooved model, energy dissipaters are the teeth. Teeth create turbulence in the flow path and give it deflection, which reduces the velocity of water and, hence, its energy. Consequently, the flow exiting over the weir enters the downstream with less energy, and severe damage downstream of the side channel does not take place. This could be an important feature of the grooved model under conditions of high discharge and energy flows, considering that they help in maintaining and stabilizing hydraulic structures. Similarly, recent research on trapezoidal-triangular labyrinth weirs (TTLWs) using soft computing techniques such as ANN and SVM also highlights the importance of geometrical configurations in energy dissipation performance. In that study, factors like relative critical depth and sidewall angle were found to play significant roles in reducing energy through flow interaction and turbulence generation (Mirkhorli et al., 2025).

Figure 8 gives the shear stress variation along the weir crest. Shear stress is amongst the main parameters concerning the stability and performance analyses of weirs. High shear stresses cause erosion and eventually damage hydraulic structures. The results show that the

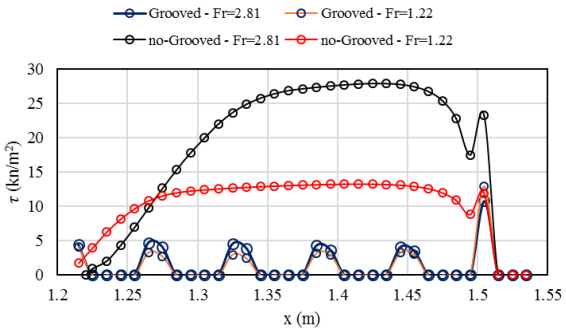

Fig. 8 Examination of shear stress on the weir

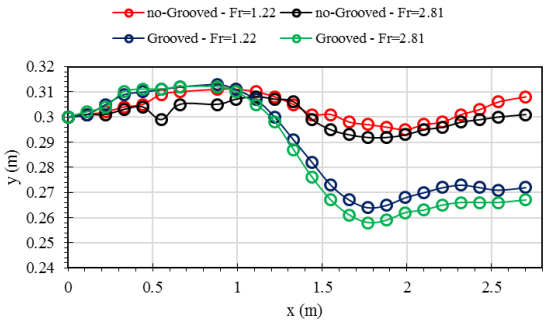

Fig. 9 Free surface profile in the two models: grooved and no-grooved

effects of grooves on shear stress along the weir crest can be well felt. The grooves on the weir crest decrease the shear stress significantly. This can be explained by the variation in flow pattern and the decrement in flow velocity within the vicinity of the weir crest. In the same way, the greater the discharge, the larger the difference in shear stresses between no-grooved and grooved models. This clearly shows that at high discharges, the shear stresses become much larger in the no-grooved model compared to the grooved model, while better performances of grooved models in energy dissipation reduce the destructive stresses. The reason why the shear stress is reduced by creating grooves on the edges of the trapezoidal side weir can be attributed to the effects of boundary layers. However, the reduction in shear stress in the case of grooves can also be attributed to the redistribution of turbulence.

Figure 9 shows the free surface profile of the flow passing via the channel and the side weir for both grooved and no-grooved models. The depth of the free surface profile decreases with the passage of the flow over the weir, then increases again. This trend is due to the variation in the flow velocity and energy with its passage over the weir. In both the models, due to the discharge of part flow through the weir, the depth of water decreases in the upstream channel. This stems from the fact that the flow overspills through the weir and thereafter drops the upstream water level. Further downstream, it again increases due to pressure recovery with an increase in the velocity of flow.

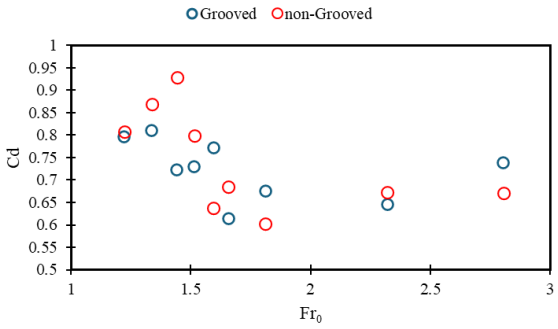

Fig. 10 Variation of C_d versus upstream Froude number

It is also seen that, in general, the flow depth is less compared to the grooved model. All this difference in flow depth is mainly because, in the grooved model, grooves dissipate some of the energy of flow and it results in an increase in flow depth, while in the no-grooved model due to the absence of these obstacles, the flow velocity increases and causes a subsequent fall in its depth.

Figure 10 shows the changes in the flow rate coefficient against the upstream Froude number. It can be inferred from this figure that at low flow rates, the flow rate coefficient in the non-groove model has increased by a maximum of 22.28% compared to the grooved model. This is while at high flow rates these changes have decreased.

Figure 11: Streamlines for different discharges. Figure 11(a) depicts the streamline of the no-grooved model, and Fig. 11(b) represents the grooved model. These figures demonstrate that in case of low discharges of $Q \leq 220$, higher flow may be passed by the grooved model compared with the no-grooved model. Again, from this grooved model, more turbulence and oscillation in streamlines have been observed than in the no-grooved model. These reveal that the grooves make the flow more turbulent. Considering the streamlines in more detail, it could be inferred that the grooved model performs better in guiding the flow and diverting it towards the weir compared to the model without grooves. This aspect, if taken into consideration, may contribute towards designing hydraulic structures since good flow guidance towards the weir prevents undesirable pressures and actual damage to the structure.

It can be observed from Figs 9 and 10 the conditions of flow downstream of the main channel. These figures depict that the variations in depth downstream are less in the case of a no-grooved model than in the grooved model. This could be because in the no-grooved model, the turbulence and energy of flow are minimal, which in turn would make the flow depth downstream gain more stability. Generally speaking, a comparison of the two models may indicate that the grooved model may be more effective for specific conditions such as low discharges and where there is a need to divert flow toward the weir. Increased turbulence, directed flow could well allow this model to find suitability for certain hydraulic applications. By contrast, the no-grooved model perhaps would run

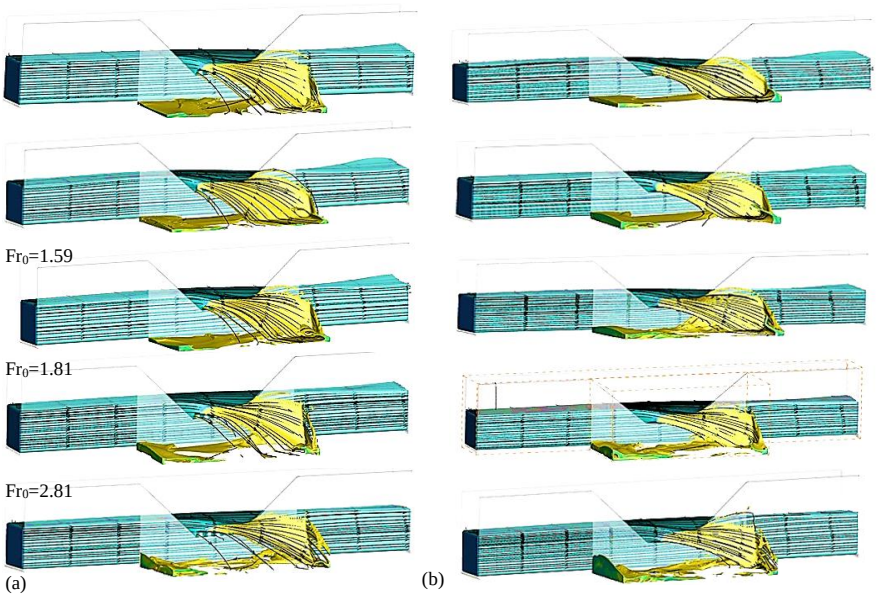

Fig. 11 Streamlines in the (a) Grooved Model, and (b) no-Grooved Model

better for those cases in which stability and a smaller fluctuation in depth are considered important, since it causes fewer changes in the downstream flow depth.

This research numerically investigates the hydraulic performance of side weirs, presenting vertical grooves, under supercritical flow conditions. The characteristics of flow were analyzed in terms of discharge coefficient, Froude number passing over the weir, shear stress, and flow surface profile along the side weir. This section will discuss the major results derived from this research work.

Numerical data are now validated with experimental results, and the error values for MAE and RMSE indices are computed as 2.8% and 3.1%, respectively. Both these error values lie within an acceptable range and reflect upon the validity of the numerical models used in the present study. This agreement qualifies that the numerical modeling in this research is good enough to simulate real flow conditions and analyze various hydraulic parameters.

The present work considered the influence of vertical grooves on hydraulic performance in side weirs operating under supercritical flow. Among the key results obtained was the reduction of the discharge coefficient in the grooved model, in respect to that without grooves. In fact, the discharge coefficient in the grooved model reduced by approximately 2.68% with respect to the discharge in the no-grooved model. This is due to the increased resistance and reduced flow velocity provided by the grooves on the weir that help in limiting the passing flow.

Furthermore, regarding the energy dissipation represented by the Froude number passing over the weir, it was found to be higher for the grooved model. Concretely, the Froude number passing over the weir for the no-grooved model was higher by 19.64% than that of grooved model; thus, showing that grooves are effective in reducing kinetic energy and, correspondingly, shear stress. The reduction of shear stress at the weir crest could contribute to less erosion and damage of hydraulic structures and, thus increase the service life of weirs.

In general, this paper demonstrated that vertical grooved side weirs could potentially offer a very efficient performance under operational and hydraulic conditions, which involve high flow energy reduction with the perspective of destructive stresses. The grooved model develops higher performance at low discharges, while the no-grooved model is maybe better for higher discharges owing to its higher discharge coefficient. The present study has a series of limitations that can be addressed and presented in future research. One of the most important of these limitations is the lack of air entry at the beginning of the simulation, which can be addressed by considering air entry with different aeration coefficients. Another limitation is that sediment transport has also been neglected.

4. CONCLUSION

This study investigates the impact of groove implementation on the hydraulic performance of sharp-edged trapezoidal side weirs, focusing on discharge coefficients and shear stress behavior. The most important results obtained from the present study can be listed as follows.

- ✓ The calculated Froude number over the weir in the no-grooved model is 19.64% higher than in the grooved model.
- ✓ In this model, the groove came to form obstacles to the flow path, causing a reduction in flow separation area and, as such, reducing the discharge coefficient. For the grooved model, with increased Froude numbers for maximum and minimum discharges, the coefficient C_d was reduced by 22.98%.

- ✓ The present study has a series of limitations that can be addressed and presented in future research. One of the most important of these limitations is the lack of air entry at the beginning of the simulation, which can be addressed by considering air entry with different aeration coefficients. Another limitation is that sediment transport has also been neglected.
- ✓ By comparing the two curves, one can clearly find out the discharge coefficient is 22.22% higher in the no-grooved model as compared to the grooved model.
- ✓ Grooved side weirs are recommended for low-flow conditions and when long-term durability is prioritized due to their lower shear stress characteristics.
- ✓ Comparing the data of the present study with the study of Tabrizi et al. (2015) showed that the numerical and laboratory data had a minimum and maximum error of 0.4 and 2.6%, respectively.

ACKNOWLEDGEMENTS

Authors can acknowledge the contribution and help of those people or institutes that do not meet the authorship criteria. The responsibility of the information released within this section is completely on the corresponding author.

CONFLICT OF INTEREST

The author must state that they have no conflicts to disclose.

AUTHORS CONTRIBUTION

E. Aminvash: Modeling; **R. Omidvar:** Writing, initial draft. **R. Danshfaraz:** review and revision; **V. Sume:** review and revision; **H. Marangoz** and **E. Yilmaz:** review and revision.

REFERENCES

Abdollahi, A., Kabiri-Samani, A., Asghari, K., Atoof, H., & Bagheri, S. (2017). Numerical modeling of flow field around the labyrinth side-weirs in the presence of guide vanes. *ISH Journal of Hydraulic Engineering*, *23*(1), 71-79. https://doi.org/10.1080/09715010.2016.1239555

Aminvash, E., & Roushangar, K. (2023). Numerical investigation of the effect of the frontal slope of simple and blocky stepped spillway with semi-circular crest on its hydraulic parameters. *Iranian Journal of Irrigation & Drainage*, *17*(1), 102-116.

Aminvash, E., Kalateh, F., Daneshfaraz, R., & Abraham, J. (2024). Investigation of the performance of soft computing methods in the hydraulic evaluation of the slot fishway on the inclined drop. *Journal of Hydraulic Structures*, *10*(1), 46-65. https://doi.org/10.22055/jhs.2024.45673.1278

Aydin, M. C., & Emiroglu, M. E. (2013). Determination of capacity of labyrinth side weir by CFD. *Flow Measurement and Instrumentation*, *29*, 1-8. https://doi.org/10.1016/j.flowmeasinst.2012.09.008

Bagherzadeh, M., Mousavi, F., Manafpour, M., Mirzaee, R., & Hoseini, K. (2022). Numerical simulation and application of soft computing in estimating vertical drop energy dissipation with horizontal serrated edge. *Water Supply*, *22*(4), 4676-4689. https://doi.org/10.2166/ws.2022.127

Daneshfaraz, R., & Ghaderi, A. (2017). Numerical investigation of inverse curvature ogee spillway. *Civil Engineering Journal (C.E.J)*, *3*(11), 1146-1156. https://doi.org/10.28991/cej-030944

Daneshfaraz, R., Aminvash, E., Esmaeli, R., Sadeghfam, S., & Abraham, J. (2020). Experimental and numerical investigation for energy dissipation of supercritical flow in sudden contractions. *Journal of Groundwater Science and Engineering*, *8*(4), 396-406. https://doi.org/10.19637/j.cnki.2305-7068.2020.04.009

Daneshfaraz, R., Aminvash, E., Ghaderi, A., Abraham, J., & Bagherzadeh, M. (2021a). SVM performance for predicting the effect of horizontal screen diameters on the hydraulic parameters of a vertical drop. *Applied Sciences*, *11*(9), 4238. https://doi.org/10.3390/app11094238

Daneshfaraz, R., Aminvash, E., Ghaderi, A., Kuriqi, A., & Abraham, J. (2021b). Three-dimensional investigation of hydraulic properties of vertical drop in the presence of step and grid dissipators. *Symmetry*, *13*(5), 895. https://doi.org/10.3390/sym13050895

De Marchi, G. (1934). "Saggio di teoria sul funzionamento degli stramazzi laterali." *L' Energia Elettrica*, *11*, Milano, Italy, 849–854 (in Italian).

Durga Rao, K. H. V., & Pillai, C. R. S. (2008). Study of flow over side weirs under supercritical conditions. *Water Resources Management*, *22*, 131-143. https://doi.org/10.1007/s11269-007-9153-4

Ghaderi, A., Dasineh, M., Abbasi, S., & Abraham, J. (2020). Investigation of trapezoidal sharp-crested side weir discharge coefficients under subcritical flow regimes using CFD. *Applied Water Science*, *10*(1), 1-12. https://doi.org/10.1007/s13201-019-1112-8

Hager, W. H. (1987). Lateral outflow over side weirs. *Journal of Hydraulic Engineering*, *113*(4), 491-504.

Henderson F. M. (1966). *Open channel flow*, Macmillan., New York.

Hyung, P. M., & Sop, R. D. (2010) Development of discharge formula for broad crested side weir. *J Korea Water Resour Assoc*, *43*(6). 525–531.

Jalili Ghazizadeh, M., Fallahi, H., & Jabbari, E. (2021). Characteristics of water surface profile over rectangular side weir for supercritical flows. *Journal of Irrigation and Drainage Engineering*, *147*(5), 04021011. https://doi.org/10.1061/(ASCE)IR.1943-4774.0001551

Kalateh, F., & Aminvash, E. (2023). Numerical simulation of the effect of channel bed slope on the hydraulic performance of sharp-crested rectangular side weir with subcritical and supercritical regimes. *Iranian Journal of Soil and Water Research*, *54*(1), 67-84. https://doi.org/10.22059/ijswr.2023.354381.669440

Kalateh, F., & Aminvash, E. (2025). Numerical investigation of aerator position effects on two-phase flow and hydraulic efficiency in morning glory spillway. *Innovative Infrastructure Solutions*, *10*(1), 10. https://doi.org/10.1007/s41062-024-01812-y

Kalateh, F., Aminvash, E., & Abraham, J. (2024a). On the effect of flow regime and slope of the channel bed on the hydraulic performance of the sharp-crested rectangular side weir: a numerical simulation. *European Journal of Environmental and Civil Engineering*, *28*(10), 2327-2344. https://doi.org/10.1080/19648189.2024.2314112

Kalateh, F., Aminvash, E., & Daneshfaraz, R. (2024b). On the hydraulic performance of the inclined drops: the effect of downstream macro-roughness elements. *AQUA—Water Infrastructure, Ecosystems and Society*, *73*(3), 553-568. https://doi.org/10.2166/aqua.2024.304

Kumar, C. P., & Pathak, S. K. (1987). Triangular side weirs. *Journal of Irrigation and Drainage Engineering*, *113*(1), 98-105. https://doi.org/10.1061/(ASCE)0733-9437(1987)113:1(98)

Maranzoni, A., Pilotti, M., & Tomirotti, M. (2017). Experimental and numerical analysis of side weir flows in a converging channel. *Journal of Hydraulic Engineering*, *143*(7), 04017009. https://doi.org/10.1061/(ASCE)HY.1943-7900.0001296

Mirkhorli, P., Bagherzadeh, M., Mohammadnezhad, H., Ghaderi, A., & Kisi, O. (2025). Energy dissipation prediction for trapezoidal–triangular labyrinth weirs based on soft computing techniques: a comparison. *ACS ES&T Water*, *5*(3), 1453-1468. https://doi.org/10.1021/acsestwater.4c01055

Nistoran, D. E. G., Simionescu, Ș. M., Cîrciumaru, G., & Chihaia, R. A. (2023). *Numerical simulations of flow over a side weir for diversion structures and water intakes.* IOP Conference Series: Earth and Environmental Science. IOP Publishing.

Seyedjavad, M., Naeeni, S. T. O., & Saneie, M. (2019). Laboratory investigation on discharge coefficient of trapezoidal piano key side weirs. *Civil Engineering Journal*, *5*(6), 1327-40. https://doi.org/10.28991/cej-2019-03091335

Simsek, O., Akoz, M. S., & Soydan, N. G. (2016). Numerical validation of open channel flow over a curvilinear broad-crested weir. *Progress in Computational Fluid Dynamics, an International Journal*, *16*(6), 364-378. https://doi.org/10.1504/PCFD.2016.10000916

Singh, R., Manivannan, D., & Satyanarayana, T. (1994). Discharge coefficient of rectangular side weirs. *Journal of Irrigation and Drainage Engineering*, *120*(4), 814-819. https://doi.org/10.1061/(ASCE)0733-9437(1994)120:4(814)

Tabrizi, H., Fatahi, R., & Ghorbani, B. (2015). Laboratory investigation on discharge coefficient of trapezoidal sharp crested side weirs. *Iranian Water Researches Journal*, *9*(1), 123-133. https://iwrj.sku.ac.ir/article_11039.html?lang=en